Analysis of AC loss contributions from different layers of HTS tapes using the A−V formulation model

Analysis of AC loss contributions from different layers of HTS tapes using the $A-V$ formulation model

A. Musso[1], M. Breschi[1], P. L. Ribani[1], F. Grilli[2]

[1]Department of Electrical, Electronic and Information Engineering, University of Bologna, Italy.
[2]Institute for Technical Physics, Karlsruhe Institute of Technology, Germany

Prepared for publication in:
IEEE Transactions on Applied Superconductivity

Abstract

This work presents a numerical model based on the definition of the scalar and vector potentials to calculate the AC losses generated in a high-temperature superconductor (HTS) coated conductor tape by an AC transport current and by an AC external magnetic field applied with a generic orientation. The material characteristics of the different layers of a reference tape are included in the model equations, which allows analyzing the differences between a model including only the superconducting layer or all layers of the coated conductor. The model is applied to study the dependence of AC losses on the amplitude of the transport current and magnetic field (applied individually or combined) and their frequency. The numerical results are compared with analytical formulations, with a second numerical model based on the *H*-formulation, and with experimental results.

The conditions at which the contribution of the non-superconducting layers to the total AC losses of the tape becomes relevant are analyzed. In particular, the dependence of losses on the frequency of the AC external magnetic field applied at different orientations, is investigated. The current density distribution computed on the conductor cross-section is used to explain the trend of the calculated losses.

Index Terms— High temperature superconducting tapes, AC losses, Current distribution, A-V formulation.

1. Introduction

The technical interest in second-generation high-temperature superconductor (HTS) tapes, formed by a stack of layers of different materials, is increasing since many studies are showing their great potential for use in magnet [1 - 3] and power applications [4 - 6]. Prototypes and full-scale devices have been developed for high field magnets [7], NMR spectrometers [8] and MRI magnets [9], as well as power cables [10], wind generators [11], SFCL [12] and SMES [13] systems. In electromagnets, current ramps and variable magnetic fields are involved, while most power applications operate with AC currents. When a coated conductor is subjected to these electrodynamic transients, time-varying magnetic fields are generated inside the material, thus giving rise to the losses. The heat produced by these losses has to be removed by the cooling system in order to safely operate the superconducting device. An increasing amount of heat enhances the cooling costs thus reducing the overall system efficiency. The correct computation of losses is therefore of great importance for the design of the cryogenic system and to avoid the insurgence of unexpected transitions from the superconductive to the resistive state.

Since measurements cannot easily be performed in all possible conditions, the use of predictive tools for AC loss computation is very useful in many situations. While analytical formulae are easy to implement and allow relatively fast calculations [14, 16], they can generally be adopted in simplified cases, which limits their applicability [17]. On the other hand, numerical models can describe more complex systems in spite of longer calculation times [18, 19]. Over the years, various finite element method (FEM) models have been developed for the analysis of the electromagnetic behaviour of HTS tapes, based on the solution of the time-dependent Maxwell's equations to compute the time evolution of the electric field and current density distributions in the conductor.

Depending on the formulations adopted for the solution of the Maxwell's equations associated to the superconductor constitutive laws, different approaches can be followed, such as the *H*-formulation [20 - 24], the $T-\Phi$ formulation [25 - 27], the $A-V$ formulation [28, 29] and the *E*-formulation [30, 31]. Various geometric approximations, 1-D [32, 33] and 2-D [34 - 37] models have been proposed to reduce the computational burden of real 3-D devices. Multidimensional approaches allow computing the losses generated in the non-superconducting layers of a tape. Since their contribution can be relevant in various operating conditions of technical interest, the choice of neglecting it, as it is often done to reduce the number of system unknowns, should be carefully evaluated.

These considerations have been proposed for both Bi-2223 tapes [38 – 41] and ReBCO coated conductors [42 – 49], even if for the latter ones the interest has been mainly focused on the impact of the ferromagnetic substrate.

This paper describes an integral model based on the *A-V* formulation to calculate AC losses in HTS tapes. The model is based on the definition of the vector potential as a function of the current density. In this field of research, the method was firstly proposed in [50] and later applied to different geometries of BSCCO tapes [51 - 53], slabs [54] and cylindrical geometries [55, 56]. To the authors' knowledge, this approach has not yet been applied to study coated conductors in two dimensions and with the presence of non-superconducting layers. In the model presented in this work, it is assumed that the self-field in the central portion of the tape can be computed assuming that the current density is independent of the tape's length (*z*-coordinate in Fig. 1). This is valid if the current redistribution length is sufficiently shorter than the tape length. This differs from the approach used in two-dimensional models for rectangular bars, which assume the conductor as infinitely long [33]. The spatial and time discretization of the tape cross-section allows one obtaining a system of ordinary differential equations, that in turn can be solved through a solver in matrix form. Unlike FEM models, the equations are written in integral form and they are solved in the conductor volume only, avoiding the discretization of the air [33]. Therefore, the number of system unknowns and the computation time are reduced. Hereupon, the spatial and time distribution of the current density is available to compute the AC losses. The model is applied to study the dependence of AC losses by transport currents and magnetic fields of different amplitude and frequency. The tape cross-section is discretized by accounting for its constituting layer materials and their electrical properties. Unlike the previous models based on the *A-V* formulation, the proposed approach allows one assessing the contribution of the individual layers to the total losses of a coated conductor. In particular, this study shows under which circumstances the losses generated in the non-superconducting layers become relevant. In fact, in certain conditions the models including only the superconducting layer or based on a 1D approximation of the tape geometry, generally adopted to reduce the computational burden, are ineffective to estimate AC losses. The model results are compared with analytical formulae, with the results of a different numerical model and with experimental results.

2. General hypothesis

As a general approach, let us consider a HTS tape connected to a power supply imposing a sinusoidal current (of frequency *f*) along the tape, $I_{Tot}(t) = I_{Amp}\, sin(2\pi f t)$. The tape, with width *w*, thickness δ and length *L*, has a rectilinear axis directed along the *z* axis of a cartesian reference system. The origin of the reference system is placed halfway along the tape length, as shown in Fig. 1. A time-dependent external magnetic field, $B_{ext}(t) = B_a\, sin(2\pi f t)$, can also be applied to the tape, in a generic direction in the *x*-*y* plane.

It is assumed that the central portion of the tape is at a sufficient distance from the tape ends, so that the distribution of the current density vector $\boldsymbol{J}$ in this section can be assumed independent of the *z*-coordinate. The same assumption can be made for the electric field $\boldsymbol{E}$ and the magnetic vector potential $\boldsymbol{A}$:

$$\begin{aligned} \boldsymbol{E}(x,y,z,t) &= E(x,y,t)\,\boldsymbol{k} \\ \boldsymbol{J}(x,y,z,t) &= J(x,y,t)\,\boldsymbol{k} \\ \boldsymbol{A}(x,y,z,t) &= A(x,y,t)\,\boldsymbol{k} \end{aligned} \tag{1}$$

In (1), $\boldsymbol{k}$ is the unit vector directed along the *z*-axis. In practical use when an electromagnetic measurement method is applied, this is equivalent to state that the tape length is significantly longer than the distance between the voltage taps soldered in the tape middle section.

The scalar potential is independent of the *x* and *y* coordinates, since it is assumed that at every location the tape cross-sections (*x*-*y planes*) are equipotential:

$$V(x,y,z,t) = V(z,t)\,\boldsymbol{k} \tag{2}$$

The tape cross-section is then discretized into *N* rectangular-shaped elements. Due to the high aspect-ratio of the tape, this shape is preferred to square elements, which would impose a finer discretization. Each layer of the tape can be discretized with a number of elements independent of that adopted for the adjacent layers. Especially at low frequencies, the currents mainly flow at the edges of the tape cross-section. Thus, a non-homogenous discretization of the superconducting layer is preferred, with a finer meshing at the edges of the tape and a coarser one in its central region. Consequently, the power dissipation per cycle per unit of tape length (in W/m) generated in the tape, takes the following expression:

$$P_{AC} = \frac{1}{T}\int_0^T \sum_{i=1}^{N} (E_i(t)\, J_i(t)\, Area_i)\, dt \tag{3}$$

where the electric field E_i and current density J_i are computed at the center of the i^{th} element of the discretization, while $Area_i$ indicates the area of each element.

3. Model equations

The electric field $\boldsymbol{E}$ is expressed as a function of the scalar electric potential V and of the magnetic vector potential $\boldsymbol{A}$:

$$\boldsymbol{E} = -\boldsymbol{\nabla} V - \frac{\partial \boldsymbol{A}}{\partial t} \tag{4}$$

By applying the assumptions reported in (1) and (2), (4) can be rewritten for each element of the system:

$$E_i(t) = -\frac{dV}{dz}(t) - \frac{dA_i}{dt}(t) \tag{5}$$

The term $\frac{dV}{dz}(t)$ is a forcing term which accounts for the voltage generated by the power source to impose the transport current of the tape. $E_i(t)$ is defined using the local form of the Ohm's law:

$$E_i(t) = \rho_i J_i(t) \tag{6}$$

where ρ_i is the electrical resistivity, whose value depends on which layer the i^{th} element belongs. If the element belongs to the superconducting layer, the power law is adopted to describe its non-linear resistivity:

$$\rho_i = \frac{E_c}{J_c}\left(\frac{|J_i|}{J_c}\right)^{n-1} \tag{7}$$

where E_c, J_c and n are the critical electric field, the critical current density and the n-value of the superconductor. The local value of the vector potential A_i can be subdivided into two different terms: A_{int_i} and A_{ext_i}. The first term takes into account the self-field of the tape, while the second one accounts for the external magnetic field. A_{int_i} can be expressed as a function of the local current density in each element of the discretization. While in [33] this relation is found for an infinitely long tape using a logarithmic kernel, the Biot-Savart law is used in this work under the following assumptions. As a first assumption, the contributions of the remaining parts of the electric circuit except for the tape, such as current leads and power supply connections, are neglected. As a second assumption, the contribution of the regions of the tape close to the tape ends, where the induced current distribution depends on the z-coordinate, is approximated by assuming the same current distribution as in the central

region. In fact, it is assumed that these lateral regions are sufficiently shorter than the central portion of the tape. These assumptions lead to the following expression:

$$A_{int_i}(t) = \frac{\mu_0}{4\,\pi}\int_{\frac{-L}{2}}^{\frac{L}{2}}\left(\sum_{j=1}^{N} Area_j \frac{J_j(t)}{\sqrt{\left(x_i - x_j\right)^2 + \left(y_i - y_j\right)^2 + (z_i - z')^2}}\right) dz' \qquad (8)$$

where the denominator represents the module of the distance between the *field point* (x_i, y_i, z_i) and the *source point* $\left(x_j, y_j, z_j\right)$. The integral of Eq. (8) can be analytically solved, which leads to:

$$A_{int_i}(t) = \frac{\mu_0}{4\,\pi}\sum_{j=1}^{N} Area_j\, J_j(t) \left|\ln\left(\sqrt{\left(x_i - x_j\right)^2 + \left(y_i - y_j\right)^2 + (z_i - z')^2} + \ (z_i - z')\right)\right|_{+\frac{L}{2}}^{-\frac{L}{2}} \qquad (9)$$

The term A_{ext_i} depends on the external magnetic field, defined as:

$$\boldsymbol{B_{ext}}(t) = \boldsymbol{B_m}\, sin(2\pi f t) = B_{mx}\, sin(2\pi f t)\, \boldsymbol{i} + B_{my}\, sin(2\pi f t)\, \boldsymbol{j} = B_{ax}(t)\, \boldsymbol{i} + B_{ay}(t)\, \boldsymbol{j}$$
$$B_m = \sqrt{{B_{mx}}^2 + {B_{my}}^2} \qquad ; \qquad \theta_{field} = \arctan\left(\frac{B_{my}}{B_{mx}}\right) \qquad (10)$$

where B_{ax} and B_{ay} are the magnetic field components, whose vector can form any angle θ_{field} with the tape's broad face. The possibility to vary the field orientation is an improvement with respect to the model reported in [32]. The expression to calculate A_{ext_i} is the following:

$$A_{ext_i}(t) = y_{c_i}\, B_{ax}(t) - x_{c_i}\, B_{ay}(t) \qquad (11)$$

where x_{c_i} and y_{c_i} are the coordinates of the center of the i^{th} element.

Then, taking the time derivative of both (9) and (11) and substituting them into (5), yields:

$$E_i(t) = $$
$$= -\frac{\partial V(z,t)}{\partial z} - \sum_{j=1}^{N} K_{i,j}\,\frac{dJ_j(t)}{dt} + x_{c_i}\frac{dB_{ay}(t)}{dt} - y_{c_i}\frac{dB_{ax}(t)}{dt} \qquad for\ i = 1{:}N$$
$$K_{i,j} = \frac{\mu_0}{4\,\pi} Area_j \left|\ln\left(\sqrt{\left(x_i - x_j\right)^2 + \left(y_i - y_j\right)^2 + (z_i - z')^2} + \ (z_i - z')\right)\right|_{+\frac{L}{2}}^{-\frac{L}{2}} \qquad (12)$$

This system of *N* differential equations includes *N* unknowns, corresponding to the current densities in every element of the discretization. However, the problem also includes a further

unknown, depending on the forcing term $\frac{\partial V(z,t)}{\partial z}$. It is convenient to rename all the system unknowns with the generic term $\psi_i(t)$:

$$\begin{cases} \psi_i(t) = J_i(t) & for\ i\ =\ 1{:}N \\ \psi_{N+1}(t) = \int_0^t \frac{\partial V}{\partial z} dt' & (N+1) - th\ unknown \end{cases} \tag{13}$$

An additional equation is then needed to solve the system reported in (12). The conservation of the total current on the tape cross-section must be imposed:

$$\sum_{j=1}^{N} I_j(t) = \sum_{j=1}^{N} Area_j\, J_j(t)\ =\ \mathrm{I}_{Tot}(t) \tag{14}$$

By applying the time derivative of the current conservation law, the terms $\psi_i(t)$ can be introduced:

$$\sum_{j=1}^{N} Area_j\ \frac{dJ_j(t)}{dt} = \sum_{j=1}^{N} Area_j\ \frac{d\psi_j(t)}{dt} = \frac{dI_{Tot}(t)}{dt} \tag{15}$$

Consequently, Eq. (12) can be rewritten by using the unknown terms described in (13) and by including (15) as the N+1 differential equation. Rewriting the $\psi_i(t)$ values at the l.h.s, yields:

$$\begin{cases} \sum_{j=1}^{N+1} Kernel_{i,j}\ \frac{d\psi_j(t)}{dt}\ = -E_i(t) + x_{c_i}\ \frac{dB_{ay}(t)}{dt} - y_{c_i}\ \frac{dB_{ax}(t)}{dt} & for\ i\ =\ 1{:}N \\ \sum_{j=1}^{N+1} Kernel_{i,j}\ \frac{d\psi_j(t)}{dt} = \frac{dI_{Tot}(t)}{dt} & for\ i = N+1 \end{cases} \tag{16}$$

which is a system of N+1 equations in N+1 unknowns. The terms $Kernel_{i,j}$ refer to the matrix *Kernel*, which has dimensions equal to (N+1)×(N+1). The first N×N terms of the matrix correspond to the $K_{i,j}$ terms reported in (12). The first N elements of the last row of the matrix $Kernel$ correspond to the terms $Area_i$. The first N elements of the last column of the matrix $Kernel$ are equal to 1, while the last element of the diagonal of the matrix $Kernel$ is null.

Finally, as reported in various studies [57, 58], the implementation of a nondimensionalization technique allows reaching a better accuracy than the dimensional analysis when solving a system of differential equations. However, it should be noted that

this topic is still debated the scientific community [59]. In the present work, the following quantities are made dimensionless:

$$J^* = \frac{J}{J_c} \quad ; \quad E^* = \frac{E}{E_c} \quad ; \quad \left(\frac{\partial V}{\partial z}\right)^* = \frac{\left(\frac{\partial V}{\partial z}\right)}{E_c} \quad ; \quad {I_{Tot}}^* = \frac{I_{Tot}}{I_{Amp}} \tag{17}$$

which leads to the following modifications of the system unknowns shown in (13):

$$\begin{cases} {\psi_i}^*(t) = {J_i}^*(t) = \dfrac{1}{J_c} J_i(x_i, y_i, t) & for\ i\ =\ 1{:}N \\ {\psi_{N+1}}^*(t) = \displaystyle\int_0^t \left(\frac{\partial V}{\partial z}\right)^* dt' = \int_0^t \frac{1}{E_c}\frac{\partial V}{\partial z} dt' & (N+1) - th\ unknow \end{cases} \tag{18}$$

Then, (16) can be rewritten in terms of the dimensionless unknowns:

$$\begin{cases} \displaystyle\sum_{j=1}^{N+1} {Kernel_{i,j}}^* \frac{d{\psi_j}^*(t)}{dt} = \\ \qquad = -{E_i}^*(t) + \dfrac{1}{E_c} x_{c_i} \dfrac{dB_{ay}(t)}{dt} - \dfrac{1}{E_c} y_{c_i} \dfrac{dB_{ax}(t)}{dt} & for\ i\ =\ 1{:}N \\ \displaystyle\sum_{J=1}^{N+1} {Kernel_{i,j}}^* \frac{d{\psi_J}^*(t)}{dt} = \frac{d{I_{Tot}}^*(t)}{dt} & for\quad i = N+1 \end{cases} \tag{19}$$

The matrix $Kernel^*$ is written starting from the matrix $Kernel$ of (16) and can be written as to:

$$Kernel^* = \begin{bmatrix} \begin{bmatrix} K^*_{1,1} & \cdots & K^*_{1,N} \\ \vdots & \ddots & \vdots \\ K^*_{N,1} & \cdots & K^*_{N,N} \end{bmatrix} & \begin{matrix} 1 \\ \vdots \\ 1 \end{matrix} \\ \dfrac{J_c}{I_{Amp}} Area_1 \quad \cdots \quad \dfrac{J_c}{I_{Amp}} Area_N & 0 \end{bmatrix} \tag{20}$$

$${K_{i,j}}^* = \frac{J_c}{E_c}\frac{\mu_0}{4\,\pi} Area_j \left| \ln\left(\sqrt{\left(x_i - x_j\right)^2 + \left(y_i - y_j\right)^2 + (z_i - z')^2 + \lambda} + (z_i - z') \right) \right|_{+\frac{L}{2}}^{-\frac{L}{2}}$$

The system (19) represents the final set of ordinary differential equations to be solved. The terms $E^*(t)$ can be easily retrieved by introducing the dimensionless quantities of (17) into (6). The term λ represents a corrective factor, introduced to avoid divergence errors occurring when the solver computes the inverse of the matrix $Kernel^*$. In particular, these problems arise from the main diagonal terms. The term λ is set through an iterative procedure, by recursively performing the same simulation while reducing the correction

factor. The smallest value found which allows convergence of the numerical is then retained for the following computations.

The initial conditions impose that the problem unknowns are null at the beginning of the simulation:

$$\psi_i^*(0) = 0 \quad for\ i = 1{:}N+1 \tag{21}$$

Once (19) is solved, (18) can be applied to retrieve the $J_i(t)$ values. Then, (6) is adopted to find the $E_i(t)$ values. Finally, it is possible to calculate the average losses during a cycle using (3).

4. Model validation

The model equations were implemented in the MATLAB software [60], but the model is suitable for an easy implementation into free alternative solvers. In order to validate the model, the geometry and electrical properties of the *SuNAM SCN04* tape were adopted. The resistivity values of conventional metals used in the simulation are reported in Table 1, as well as the parameters of superconductor power law, computed from experimental measurements. The tape geometrical parameters are shown in Fig. 2 [61]. The tape length is set to 10 cm, in order to analyse the measurements carried out for this study.

It is worth noting that A_{int_i} depends on the tape length (see Eq. (8)). A preliminary analysis was performed in this regard, showing that the calculated AC losses converge for tape lengths greater than or equal to 10 cm. The buffer layer was neglected in the model: given its small thickness, its impact on the AC losses is assumed as minor. After a convergence analysis performed for the calculation of the transport current losses, the numbers of points to discretize the superconducting layer along its width and thickness were set to 200 and 4, respectively. The total number of elements to discretize the cross-section of the other layers was set to 390, distributed between the different layers.

Three main sets of simulations were performed. In the first set, the losses due to a sinusoidally varying transport current were analysed. In the second set, the study was focused on analysing the losses due to a sinusoidal magnetic field, applied in phase with the transport current and with different orientations with respect to the tape's broad face. In the third set of simulations, the impact of the combined action of transport current and applied

magnetic field was analysed. In all sets of simulations, parametric studies were performed to assess the impact of both frequency and field/current amplitude on the overall losses.

The duration of the simulated number of periods of the sinusoidal signals considered in the simulations was set to 2. It was verified that the system already reached its regime conditions during the second period, which was therefore selected in order to compute the losses through the integral reported in (3). The integration time step was set in all simulations to 1/100 of the period. The corrective term λ of (19) is set to $2.5 \cdot 10^{-9}$, since it is the lowest value to ensure the solver convergence.

In order to identify the contribution of all tape layers to the total losses, two different types of analyses were performed with the model based on the *A-V* formulation. In the first case, referred to as "*Whole_Tape*", all layers of the tape cross-section were included in the model. In the second case instead, named "*SC_only*", only the superconducting layer was implemented in the model and the other layers were neglecred. Three methods were adopted for the model validation. As a first approach, the model results were compared to those of a distinct numerical model based on the 2D approximation of the *H*-formulation [20 - 24]. This second model was implemented in the COMSOL Multiphysics environment [62]. Furthermore, the numerical results were compared with those obtained through analytical formulae available in the literature. Finally, the model results were compared to experimental data obtained on the same tape.

Throughout the paper, when the dependency on the amplitude of the transport current or the magnetic field is analysed, the average power dissipation over a full cycle is presented in units of W/m. Instead, when the loss dependency on frequency is studied, the overall losses per cycle are presented in terms of J/m. The average power dissipation can easily be computed by multiplying the AC loss energy per cycle by the frequency. Hereafter, the tape current is expressed as a dimensionless ratio of the transport current amplitude to the tape critical current: $I_m = \frac{I_{Amp}}{I_c}$.

4.1. Transport AC losses

The losses due to a sinusoidal transport current are reported in Figure 3(a) for different I_m values at a frequency of 50 Hz. As a first validation, the difference between the results obtained with the model based on the *H*-formulation is below 20% at low amplitudes, decreasing below 2% when I_m approaches I_c. The results of the analytical formula valid for a thin strip of finite width (see [14]) are also reported in the plot. The numerical results fit

well the analytical ones, although some discrepancies can be observed at particularly small and large transport current values. In fact, the analytical formula adopts the critical state model for the superconductor [63] instead of the power law, reported in (7). It has been proven that increasing the *n-value* used in the simulation, the agreement between the two computation methods improves.

The non-superconducting layers of the tape do not generate significant dissipation since the differences between the "*Whole_Tape*" and "*SC_only*" numerical curves are minor (below 0.5 %).

The comparison with the experimental results is also shown in the plot. The experiments were performed on the same tape as that sketched in Fig. 2. The experimental setup, the measurement procedure and the post-processing methodology adopted to treat the acquired signals are described in detail in [64].

The experimental data generally exhibit greater values than the numerical ones, especially for low values of I_m (more than 2 times higher), while they tend to converge with the other curves at high current amplitudes (the differences get lower than 30% when $I_m >$ 0.6). The discrepancies at low currents can be ascribed to local variations of the critical current density across the tape width. At low transport current amplitudes, the penetration of the induced currents remains limited to the tape sides, where the current density can be lower. The proposed model does not account for the critical current density inhomogeneities, which might be a source of discrepancy with the experimental data, as shown in [65]. Another possible explanation for this discrepancy can be ascribed to the adoption in the model of a field independent *J*c value. In practice, the tape self-field can locally modify the J_c within the tape, thus affecting the measured AC losses. Future developments will aim to include a field-dependent J_c in the model equations.

4.2. Magnetization losses

Figure 3(b) reports the results of the model validation for the case of a sinusoidal magnetic field applied perpendicular to the tape, with variable field amplitude (B_a) and frequency set to 50 Hz. The difference between the results obtained with the model based on the *H*-formulation is below 15% when B_a = 10 mT, decreasing below 1% already at $B_a >$ 0.1 T. The analytical results for this analysis were computed by means of the formula developed for a thin strip in perpendicular field, presented in [15, 16]. The change in the curve slope for field amplitudes around 50 mT indicates the condition at which themagnetic saturation

is reached in the tape. The numerical and the analytical results are in good agreement, although they start to diverge at high field amplitudes.

The numerical results obtained in the "*Whole_tape*" case indicate losses at high fields slightly greater than those obtained in the "*SC_only*" case, with a maximum difference of 13% with B_a = 2 T. This can be explained as an increasing contribution of the non-superconducting layers to the total losses. These aspects will be analysed more thoroughly in the next section.

4.3. AC losses due to a combination of time-varying transport current and magnetic field

Figure 3(c) presents the losses generated in the tape by the combination of a variable transport current and a sinusoidal magnetic field applied perpendicular to the tape. In this study, the current amplitude is varied, while the perpendicular field amplitude is set to 0.1 T; the frequency of both AC sources is set to 50 Hz. The curves obtained with the *A-V* and the *H* formulations are in very good agreement (the discrepancies are below 0.5%), thus providing a further validation of the numerical model. The difference between the results of the *A-V* model obtained in the "*Whole_tape*" and "*SC_only*" cases remains below 1%, which indicates that the losses generated in the non-superconducting layers have a minor impact.

As expected, the combination of the two AC sources determines greater losses than those found for their separate application. It is worth noting that the power increases by 2.9 W/m when the current rises from its lower (I_m = 0.1) to its higher value (I_m = 1). In comparison, the increase obtained between the same amplitudes in absence of the magnetic field (Fig. 3 (a)) is around 0.3 W/m. When both AC sources are applied simultaneously, the transport current flows in conditions which significantly differ from those obtained for the analyses reported in Fig. 3(a). As a matter of fact, the presence of a magnetic field produces a certain distribution of induced currents within the tape. For a field amplitude of 0.1 T, for instance, the tape is fully penetrated by the field and its induced currents. Thus, when both AC sources are present, the transport current superimposes to the current distribution generated by the field variations and its contribution to the dissipated power gets higher [66].

Finally, Table II shows some examples of computation times for this integral approach, in comparison with those obtained with the *H*-formulation (both found on a computer equipped with an Intel Xeon E5-2650 v3 CPU and 64 GB of RAM). Three cases are reported, in which the AC sources are either applied separately or act simultaneously. The computations with the *A-V* formulation are 2.4 to 4.8 times faster than those based on

the *H*-formulation. However, this comparison is affected by the greater number of degrees of freedom required to achieve convergence in the FEM model. In fact, the stacked configuration requires the spatial discretization along the tape width to be the same for all layers, which does not apply for the integral model. In the model based on the *H*-formulation, the superconducting layer was discretized with 180 elements while all the other layers were discretized with 4320 elements, distributed between the different layers. Moreover, the FEM model requires discretizing the air, which enhances the computation times. Lately, the so-called *H*-φ model was proposed, which can partially reduce this drawback [67].

5. Analysis of the contribution of individual tape layers.

The contribution of the individual layers to the total losses of the tape is analysed in this section. The operating conditions which determine a remarkable contribution of the non-superconducting layers of the tape to the total tape losses are presented in this section.

5.1. Losses in individual tape layers due to a perpendicular magnetic field

Figure 4 shows the losses obtained by varying the perpendicular field frequency with an amplitude set to 0.1 T. All curves overlap at low frequencies. For frequencies higher than 100 Hz, while the "*SC_only*" curve remains essentially frequency independent, the "*Whole_tape*" curve exhibits a significant rise. For a better understanding of this trend, Fig. 5 shows the magnetization losses generated in each layer of the tape. The losses in the superconducting layer are frequency-independent up to about 1 kHz; above this threshold value, they start to decrease. The losses generated in the other layers increase with frequency and reach remarkable values at frequencies of some kHz (especially for the copper layers). In these conditions, their contribution to the total losses generated in the tape exceeds 50%. For a better insight in the underlying physical phenomena, Figure 6 depicts the J/J_c distribution in the cross-section of the superconducting layer, computed for different frequencies (10 Hz, 100 Hz, 1 kHz and 10 kHz) with a perpendicular field amplitude of 0.1 T. Various instants of the field cycle are shown, corresponding to $\omega t = \frac{5}{2}\pi$ (a) and $\omega t = 3\,\pi$ (b). These time instants are all included in the second period, since the regime conditions are not yet reached during the first one. The plots reported on the left refer to the "*Whole_tape*" model, although only the current distribution in the superconducting layer is presented. The plots reported on the right correspond to the "*SC_only*" model. The thickness of the superconductor was finely discretized (8 elements) in order to obtain a sufficiently precise

representation of the current density fronts at different time instants. However, for the mere AC loss calculation, such fine discretization is not necessary. Both Figs 6(a) and 6(b) show that there are no significant differences between the current density distributions obtained with the two models for frequencies up to 1 kHz. When the induced current distributions are the same for the different cases, the losses obtained are equal. This result is consistent with the frequency independence of the AC losses in the superconducting layer at these frequency values, as displayed in Fig. 5. When the frequency overcomes 1 kHz, some discrepancies between the two models can be observed. In particular, the "*Whole_tape*" case results in lower values of the J/J_c ratio (and therefore of the amplitude of induced currents) in the central area of the superconductor as compared to the "*SC only*" case. This indicates that the induced currents can no longer penetrate this layer completely. This might be due to the fact that at very high frequencies the electric field rises to significant values, and therefore the induced currents start following different paths, passing through the metallic layers of the tape. Since lower induced current amplitudes determine lower values of the losses, the current distributions shown in Fig. 6 prove that the losses decrease in the superconducting layer above 1 kHz. Instead, it can be inferred that the induced currents increase in the normal layers, which produce a greater loss contribution. Thus, for the computation of magnetization losses, neglecting the non-superconducting layers of a tape becomes a too rough approximation when the frequency exceeds 1 kHz. The same outcomes are verified for all the other instants. It is worth noting how the induced currents shift from the outer to the inner part of the tape during time. The sign of the new induced currents changes according to the increasing or decreasing time variations of the external field.

5.2. Losses in individual tape layers due to a magnetic field of different orientations

The model was then applied to calculate the magnetization losses generated by a variable magnetic field applied with different orientations with respect to the tape broad face. In order to reach convergence also for nearly parallel field orientations, the spatial discretization of the HTS layer was refined to reach 8 elements along its thickness. Figure 7 shows the magnetization losses for different θ_{field} angles, with variable field amplitudes at a frequency set to 50 Hz. By reducing the incidence angle at constant B_a, the losses are lowered. For sufficiently wide angles, the losses do not greatly differ from the perpendicular case; on the contrary, when the angle of incidence approaches the parallel case, the losses are drastically reduced by several orders of magnitude. There is no significant difference in the results obtained with the "*Whole_tape*" or "*SC_only*" models, except for the parallel

case. In this case, the discrepancy between the two cases is significant: the contribution of the non-superconducting layers never drops below 50%.

Fig. 8 shows the magnetization losses for a field with different orientations and frequencies and a fixed amplitude of 0.1 T. The losses found with the "*SC_only*" model are almost frequency-independent. For the "*Whole_tape*" model instead, all curves converge with the "*SConly*" case at low frequencies and then rise when the frequency exceeds a threshold value. This threshold is in the order of hundreds of Hz for all cases, except for the parallel field case, where the "*WholeTape*" curve diverges already for frequencies of tens of Hz. In this case, the impact of the non-superconducting layers is significant even at low frequencies, becoming predominant (> 50%) around 600 Hz, and approaching 100% of the total losses for frequencies above 1 kHz. Indeed, for parallel field the thicknesses of the different layers determine the extent of the induced currents, and therefore the losses generated in each layer. Since the metallic layers are thicker than the superconducting one, their contribution becomes relevant. This phenomenon is enhanced at high frequencies [48]. In these conditions it is therefore of great importance to include the non-superconducting layers in the calculation of the magnetization losses due to parallel fields.

Conclusions

A numerical analysis of the AC losses in HTS tapes using an integral form of the *A-V* formulation is presented in this work. The model assumes that in the central portion of the tape the system variables are independent of the *z*-coordinate, thus simplifying the equations and reducing the computational burden. The model was applied to the calculation of the transport AC losses, the magnetization losses and for a combination of the two AC sources. Unlike previous works, this model applies the integral model to coated conductors' geometries. The model was validated against a second numerical model based on the *H*-formulation, as well as analytical formulae and experimental results.

The model allows one computing the losses generated in all layers of the tape, in order to quantify their relevance in different conditions. The analysis of the current density distribution on the conductor cross-section is also reported to explain the trend of the computed losses. It is concluded that the contribution to the total losses of the non-superconducting layers is enhanced when the frequency of the applied external magnetic field exceeds 1 kHz. In turns, the induced currents in the superconducting layer are reduced, producing lower losses. Furthermore, if the magnetic field is parallel to the tape main face, the impact of non-superconducting layers is already relevant at frequencies of tens of Hz.

For these conditions, the simulation of the superconducting layer only, a simplification often adopted in the literature to reduce the computational burden, is not acceptable for a correct assessment of the AC losses. For all the other cases, considering only the superconducting layer provides a good approximation of the total tape losses.

References

[1] A. Ballarino, "*Prospects for the use of HTS in High-field Magnets for Future Accelerator Facilities*", *Proc. 5th Int Part. Accel. Conf, vol. IPAC2014*, pp. 6 pages, 2014.

[2] H. Maeda and Y. Yanagisawa, "*Recent Developments in High-Temperature Superconducting Magnet Technology (Review)*", *IEEE Trans. Appl. Supercond*., vol. 24, no. 3, pp. 1–12, Jun. 2014.

[3] D. Uglietti, "*A review of commercial high temperature superconducting materials for large magnets: from wires and tapes to cables and conductors," Supercond. Sci. Technol.,* vol. 32, no. 5, p. 053001, Apr. 2019.

[4] J. X. Jin et al., "*Enabling High-Temperature Superconducting Technologies Toward Practical Applications", IEEE Trans. Appl. Supercond*., vol. 24, no. 5, pp. 1–12, Oct. 2014.

[5] X.-Y. Xiao *et al.*, "*HTS Applied to Power System: Benefits and Potential Analysis for Energy Conservation and Emission Reduction"*, *IEEE Trans. Appl. Supercond.,* vol. 26, no. 7, pp. 1–9, Oct. 2016.

[6] J. X. Jin et al., "*HTS Power Devices and Systems: Principles, Characteristics, Performance, and Efficiency", IEEE Trans. Appl. Supercond.,* vol. 26, no. 7, pp. 1–26, Oct. 2016.

[7] S. Hahn *et al.,* "*45.5-tesla direct-current magnetic field generated with a high-temperature superconducting magnet*," *Nature*, vol. 570, pp. 496–499, Jun. 2019.

[8] J. Bascunan *et al.*, "*A new High-Temperature Superconducting (HTS) 700-MHz insert magnet for a 1.3-GHz LTS/HTS NMR magnet," IEEE Trans. Appl. Supercond*., vol. 23, no. 3, p. 4400304, Jun. 2013.

[9] B. J. Parkinson *et al.*, "*Development of a cryogen free 1.5 T YBCO HTS magnet for MRI*," *IEEE Trans. Appl. Supercond.,* vol. 23, no. 3, p. 4400405, Jun. 2013.

[10] O. Maruyama *et al., "Development of RBCO HTS power cables," Physics Procedia*, vol. 36, pp. 1153-1158, Jun. 2012.

[11] A. Bergen *et al., "Design and in-field testing of the world's first ReBCO rotor for a 3.6 MW wind generator," Supercond*. Sci. Technol., vol. 32, no. 12, p. 125006, Oct. 2019.

[12] C. A. Baldan *et al., "Performance of modular SFCL using REBCO coated conductor tapes under repetitive overcurrent tests," IEEE Trans. Appl. Supercond*., vol. 26, no. 3, p. 5401905, Apr. 2016.

[13] J. Ciceron *et al., "Test in Strong Background Field of a Modular Element of a REBCO 1 MJ High Energy Density SMES," IEEE Trans. Appl. Supercond*., vol. 28, no. 8, p. 5701005, Jun. 2018.

[14] W. T. Norris, "*Calculation of hysteresis losses in hard superconductors carrying AC isolated conductors and edges of thin sheets,*" *J. Phys. Appl. Phys*., vol. 3, no. 4, pp. 489–507, Apr. 1970.

[15] E. H. Brandt, "*Type-II-superconductor strip with current in a perpendicular magnetic field,*" *Phys. Rev. B*, vol. 48, no. 17, pp. 893–906, Nov. 1993.

[16] M. R. Halse, "*AC face field losses in a type II superconductor*," *Journ. of Phys. D: Appl. Phys.,* vol. 3, no. 5, pp. 717–720, May 1970.

[17] G. P. Mikitik *et al.*, '*Analytical Methods and Formulas for Modeling High Temperature Superconductors,' IEEE Trans. On Appl. Supercond.*, vol. 23, no. 2, p. 8001920, Apr. 2013.

[18] F. Grilli *et al.*, '*Computation of Losses in HTS Under the Action of Varying Magnetic Fields and Currents,' IEEE Trans. On Appl. Supercond.*, vol. 24, no. 1, p. 8200433, Feb. 2014.

[19] F. Grilli, '*Numerical Modeling of HTS Applications'*, *IEEE Trans. On Appl. Supercond.*, vol. 26, no. 3, p. 0500408, Apr. 2016.

[20] Z. Hong *et al*., "*Numerical solution of critical state in superconductivity by finite element software*," *Supercond. Sci Technol.*, vol. 19, pp. 1246-1252-24, Oct. 2006.

[21] R. Brambilla *et al.*, '*Development of an edge-element model for AC loss computation of high-temperature superconductors,' Supercond. Sci Technol.*, vol. 20, pp. 16-24, Nov. 2006.

[22] D. N. Nguyen *et al.*, '*A new finite-element method simulation model for computing AC loss in roll assisted biaxially textured substrate YBCO tapes,*' *Supercond. Sci Technol.*, vol. 23, no. 2, p. 025001, Dec. 2009.

[23] B. Shen *et al.*, '*Overview of H-Formulation: A Versatile Tool for Modeling Electromagnetics in High-Temperature Superconductor Applications,' IEEE Access*, vol. 8, pp. 100403 - 100414, May 2020.

[24] B. Shen *et al.*, '*Review of the AC loss computation for HTS using H formulation,' Supercond. Sci. Technol.,* vol. 33*,* no. 3, p. 033002, Feb. 2020.

[25] N. Amemiya*.*, '*Numerical modelings of superconducting wires for AC loss calculations'*, *Physica C.*, vol. 310, issue 1-4, pp. 16-29, Dec. 1998.

[26] F. Grilli *et al.*, '*Finite-Element Method Modeling of Superconductors: From 2-D to 3-D'*, *IEEE Trans. On Appl. Supercond.*, vol. 15, no. 1, pp. 17-24, Mar. 2005.

[27] A. Stenvall *et al.*, "*Programming finite element method based hysteresis loss computation software using non-linear superconductor resistivity and T- φ formulation,*" *Supercond. Sci Technol.*, vol. 23, p. 075010, Nov. 2010.

[28] A. Stenvall *et al.*, "*An eddy current vector potential formulation for estimating hysteresis losses of superconductors with FEM*," *Supercond. Sci Technol.*, vol. 23, p. 125013, Nov. 2010.

[29] N. Nibbio *et al.*, '*Finite element method simulation of AC loss in HTS tapes with B-dependent E-J power law,' IEEE Trans. On Appl. Supercond.*, vol. 11, no. 1, p. 2631, Mar. 2001.

[30] J. K. Sykulsk *et al.* "*Modelling HTc superconductors for AC power loss estimation,*" *IEEE Trans. On Magnetics*, vol. 33, no. 2, pp. 1568-1571, Mar. 1997.

[31] J. K. Sykulsk *et al.* "*2D modeling of field diffusion and AC losses in high temperature superconducting tapes,*" *IEEE Trans. On Magnetics*, vol. 36, no. 4, pp. 1178-1182, Jul. 2000

[32] S. Stavrev *et al.*, "*Comparison of the AC losses of BSCCO and YBCO conductors by means of numerical analysis*," *Supercond. Sci Technol.*, vol. 18, pp. 1300-1312, Aug. 2005.

[33] S. Otten *et al.,* "*Simple and Fast Method for Computing Induced Currents in Superconductors Using Freely Available Solvers for Ordinary Differential Equations*," *IEEE Trans. On Appl. Supercond*, vol. 29, no.8, p. 8202008, Dec. 2019.

[34] E. Vinot *et al.* "*Different Formulations to Model Superconductors,*" *IEEE Trans. On Appl. Supercond.*, vol. 36, no. 4, pp. 1226-1229, Jul. 2000.

[35] N. Enomoto., '*Electromagnetic field analysis of rectangular high Tc superconductor with large aspect ratio,' Physica C.*, vol.s 412-414, Part 2, pp. 1050-1055, Oct. 2004.

[36] F. Grilli *et al.*, '*Modeling High-Temperature Superconducting Tapes by Means of Edge Finite Elements,*' *IEEE Trans. On Appl. Supercond.*, vol. 17, no. 2, p. 3155, Jun. 2007.

[37] E. Pardo *et al.*, "*Numerical simulations of the angular dependence of magnetization AC losses: coated conductors, Roebel cables and double pancake coils*," *Supercond. Sci Technol.*, vol. 18, p. 014008, Oct. 2011.

[38] S. Stavrev *et al.*, '*Eddy current self-field loss in Bi-2223 tapes with a.c. transport current,' Physica C*, vol. 307, pp. 105-116, Oct. 1998.

[39] S. Stavrev *et al.*, '*Frequency dependence of AC loss in Bi-2223/Ag-sheathed tapes,' Physica C*, vol. 310, pp. 86-89, Dec. 1998.

[40] C. M. Friend *et al.*, '*A European Project on the AC Losses of Bi-2223 Tapes for Power Applications,' IEEE Trans. On Appl. Supercond.*, vol. 9, no. 2, pp. 1165-1168, Jun. 1999.

[41] W. Chen *et al.*, '*AC Loss of Bi-2212 Round Wire at Wide Frequency Ranges up to 500 kHz,' IEEE Trans. On Appl. Supercond.*, vol. 31, no. 1, p. 6400110, Jun. 2021.

[42] H. Lee *et al.*, '*Estimation of the AC loss of a YBCO coated conductor with metal substrate by Using Numerical calculation,' IEEE Trans. On Appl. Supercond.*, vol. 15, no. 2, pp. 1558 - 1561, Jun. 2005.

[43] D. Miyagi *et al.*, '*Measurement of magnetic properties of Ni-alloy substrate of HTS coated conductor in LN_2,' Physica C*, vol. 468, pp. 1743-1746, Sept. 2008.

[44] F. Gomory *et al.,* "*AC losses in coated conductors*," *Supercond. Sci. Technol*., vol. 23, no. 3, p. 034012, Feb. 2010.

[45] S. Li *et al.,* "*Transport AC losses of a second-generation HTS tape with a ferromagnetic substrate and conducting stabilizer*," *Supercond. Sci. Technol*., vol. 28, no. 12, p. 125011, Nov. 2015.

[46] G. Liu *et al.*, '*Experimental and numerical study of frequency-dependent transport loss in YBa 2 Cu 3 O 7–δ coated conductors with ferromagnetic substrate and copper stabilizer*', *J. Appl. Phys.*, vol. 121, no. 24, p. 243902, Jun. 2017.

[47] B. Shen *et al.*, '*Investigation and comparison of AC losses on stabilizer-free and copper stabilizer HTS tapes,' Physica C: Superconductivity and its applications*, vol. 541, pp. 40-44, Aug. 2017.

[48] J. Ma *et al.*, "*A temperature-dependent multilayer model for direct current carrying HTS coated-conductors under perpendicular AC magnetic fields*," *Supercond. Sci. Technol*., vol. 33, no. 4, p. 045007, Feb. 2020.

[49] P. Zhou *et al.*, "*Transition frequency of transport ac losses in high temperature superconducting coated conductors*," *J. Appl. Phys.*, vol. 126, p. 063901, Aug. 2019.

[50] E. H. Brandt, "*Thin superconductors in a perpendicular magnetic AC field: General formulation and strip geometry*," *Phys. Rev. B*, vol. 49, no. 13, pp. 9024–9040, 1994.

[51] S. Stavrev *et al.* "*Comparison of Numerical Methods for Modeling of Superconductors,*" *IEEE Trans. On Magnetics*, vol. 38, no. 2, pp. 849-852, Mar. 2002.

[52] H. Tonsho *et al.*, '*Theoretical and experimental study on AC loss in HTS tape in AC magnetic field carrying AC transport current,' IEEE Trans. On Appl. Supercond.,* vol. 13, no. 2, p. 2368, Jun. 2003.

[53] M. Vojenciak *et al.*, '*Losses in Bi-2223/Ag tape at simultaneous action of AC transport and AC magnetic field shifted in phase,' Journal of Physics: Conference Series,* vol. 43, pp. 63-66, Sept. 2005.

[54] M. C. Bouzo *et al.,* "*Modelling of coupling between superconductors of finite length using an integral formulation*," *Supercond. Sci. Technol*., vol. 17, no. 10, pp. 1103-1112, Jul. 2004.

[55] D. X. Chen *et al.,* "*AC susceptibility and critical-current densities in sintered* $YBa_2Cu_3O7_{-\delta}$ *superconductors*," *Appl. Phys. Lett*., vol. 89, no. 7, p. 072501, Aug. 2006.

[56] M. Elbaa *et al.,* "*Analytical modeling of an inductor in a magnetic circuit for pulsed field magnetization of HTS bulks*," *IEEE Trans. Appl. Supercond*, vol. 28, no. 4, p. 8201306, Jun. 2018.

[57] A. A. Sonin, "*The physics basis of dimensional analysis*," MIT Cambridge, Massachusetts, United States, 1997

[58] D. G. Schaeffer *et al.,* "*Nondimensionalization and Scaling. In: Ordinary Differential Equations: Basics and Beyond,*" *Texts in Applied Mathematics*, *Springer*, vol. 65, New York, United States, 2016.

[59] J. F. Sánchez Pérez *et al.,* "*Searching fundamental information in ordinary differential equations. Nondimensionalization technique*," *PLoS ONE 12,* vol. 10, p. 0185477, Oct. 2017.

[60] MATLAB. Version 2020a, *The Math Works Inc*., Natick, Massachusetts, United States, 2020.

[61] *http://i-sunam.com/home/en_product,1,3,1,1,1*

[62] COMSOL Multiphysics® v. 5.5, *www.comsol.com*. *COMSOL AB*, Stockholm, Sweden, 2020.

[63] C. P. Bean "*Magnetization of High-Field Superconductors*," *Reviews of Modern Physics. American Physical Society*, vol. 36, no. 1, pp. 31–39, Jan. 1964.

[64] M. Breschi, F. Filicori, A. Musso and G. Pasini., "*An electromagnetic method for measuring AC losses in HTS tapes without lock-in amplifier*," *Journal of Physics: Conference Series*, vol. 1559, no.1, Jun. 2020.

[65] M. Solovyov *et al.*, '*Non-uniformity of coated conductor tapes,' Supercond. Sci Technol.*, vol. 26, no.11, p. 115013, Oct. 2013.

[66] E. Pardo *et al.*, '*Current distribution and ac loss for a superconducting rectangular strip with in-phase alternating current and applied field,' Supercond. Sci Technol.*, vol. 20, no.4, pp. 351-364, Mar. 2007.

[67] A. Arsenault *et al., "Implementation of the H-ϕ formulation in COMSOL Multiphysics for simulating the magnetization of bulk superconductors and comparison with the H-formulatio*n," arXiv:2006.13784.

Figures

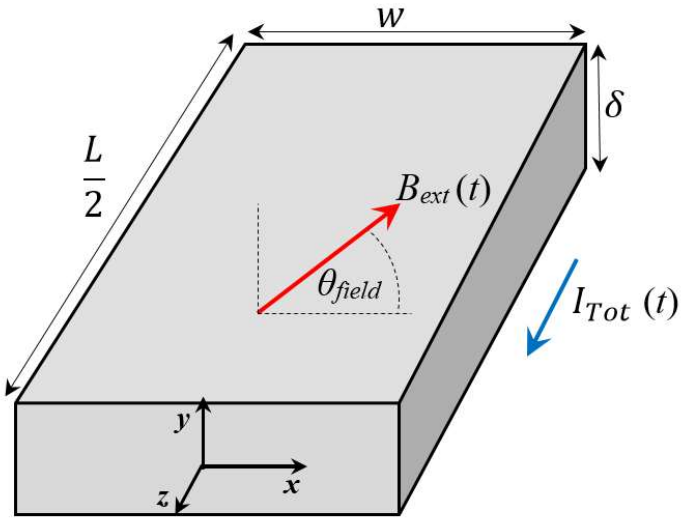

Figure 1. Reference system and geometrical parameters for an HTS tape subjected to AC conditions.

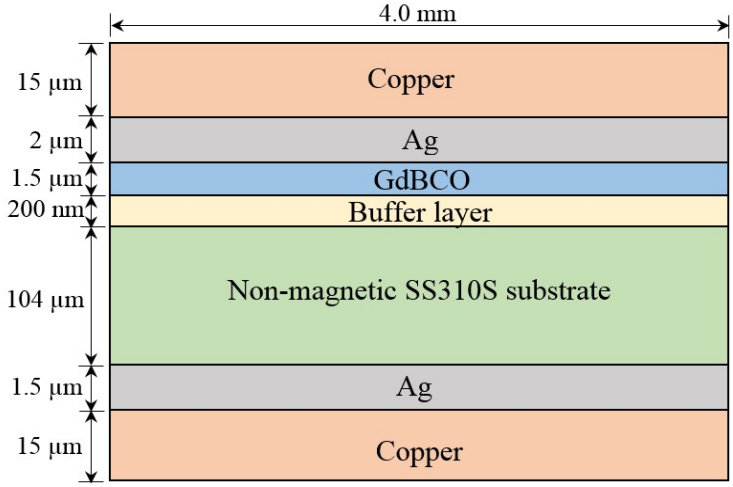

Figure 2. Cross-section of the *SuNAM SCN04* tape. The figure is not in scale.

Parameter	***Unit***	***Value***
I_c (77 K , E_c = 1 µV/cm)	[A]	242
n- value (77 K , E_c = 1 µV/cm)		43
ρ_{Cu}	[Ω m]	1.97e-9
ρ_{Ag}	[Ω m]	2.7e-9
$\rho_{Substrate}$	[Ω m]	7.24e-7

Table 1. Electrical parameters of the *SuNAM SCN04* tape.

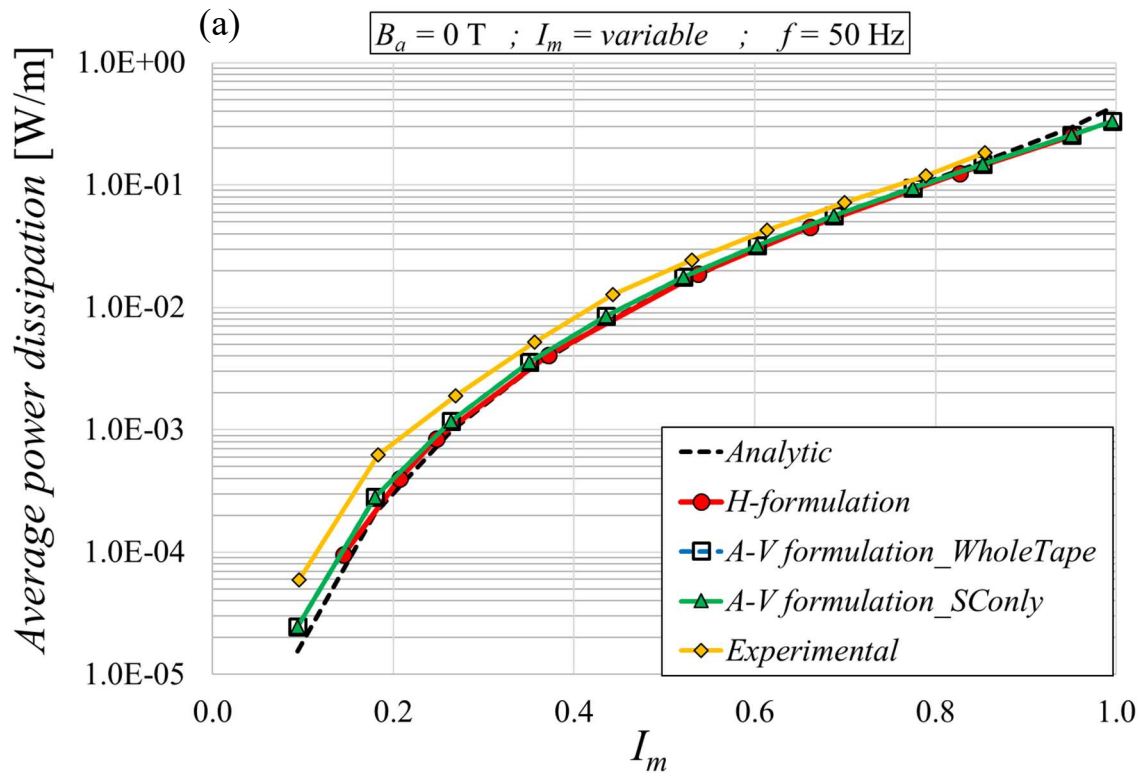
(a)
B_a = 0 T ; I_m = variable ; f = 50 Hz
Average power dissipation [W/m]
1.0E+00
1.0E-01
1.0E-02
1.0E-03
1.0E-04
1.0E-05
0.0
0.2
0.4
0.6
0.8
1.0
I_m
Analytic
H-formulation
A-V formulation_WholeTape
A-V formulation_SConly
Experimental

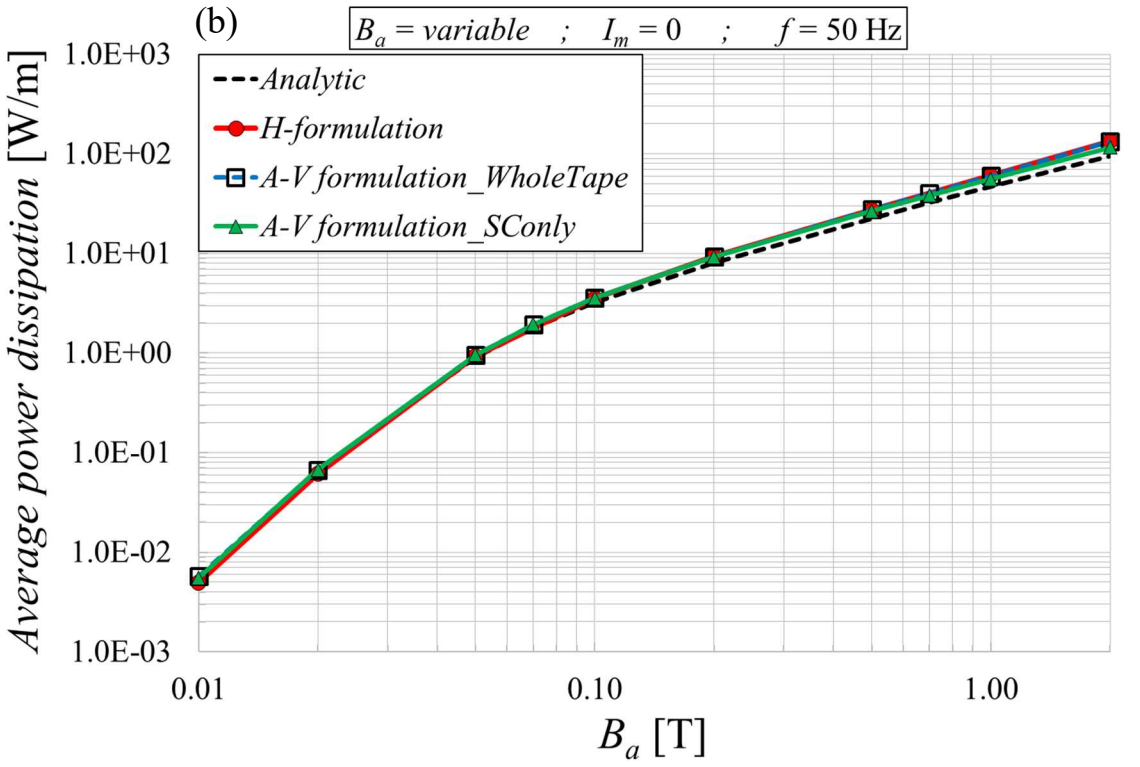
(b)
B_a = variable ; I_m = 0 ; f = 50 Hz
Average power dissipation [W/m]
1.0E+03
1.0E+02
1.0E+01
1.0E+00
1.0E-01
1.0E-02
1.0E-03
0.01
0.10
1.00
B_a [T]
Analytic
H-formulation
A-V formulation_WholeTape
A-V formulation_SConly

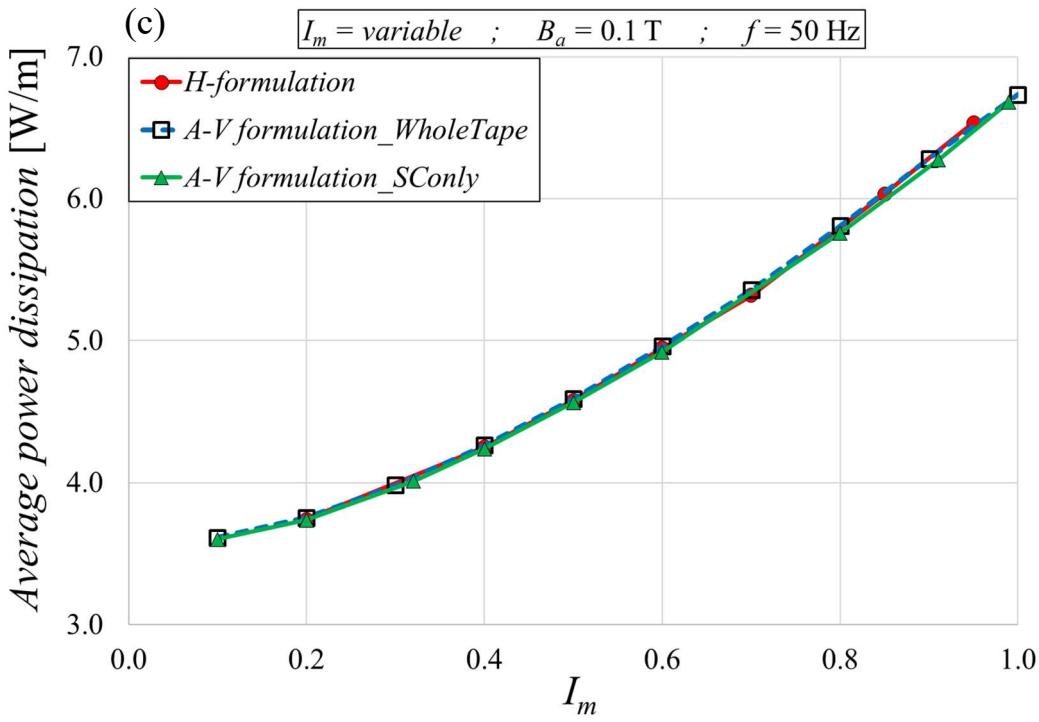

Figure 3. Average power dissipation in the *SuNAM SCN04* tape due to different sources, computed with different methodologies. (a) Transport current only: varying I_m with f = 50 Hz. (b) Perpendicular field only: varying the field amplitude with f = 50 Hz. (c) Both AC sources together: varying I_m with a field amplitude of 0.1 T and f = 50 Hz.

Parameters			***Simulation time***		***Speed-up***
I_m	B_{ay}	f	*A-V formulation*	*H-formulation*	
	[T]	[Hz]	[s]	[s]	
0.7	0.0	50	158	759	4.8
0.0	0.1	50	320	962	3.0
0.7	0.1	50	375	901	2.4

Table 2. Simulation times for the *A-V* formulation and the *H*-formulation to compute AC losses with the same operating parameters.

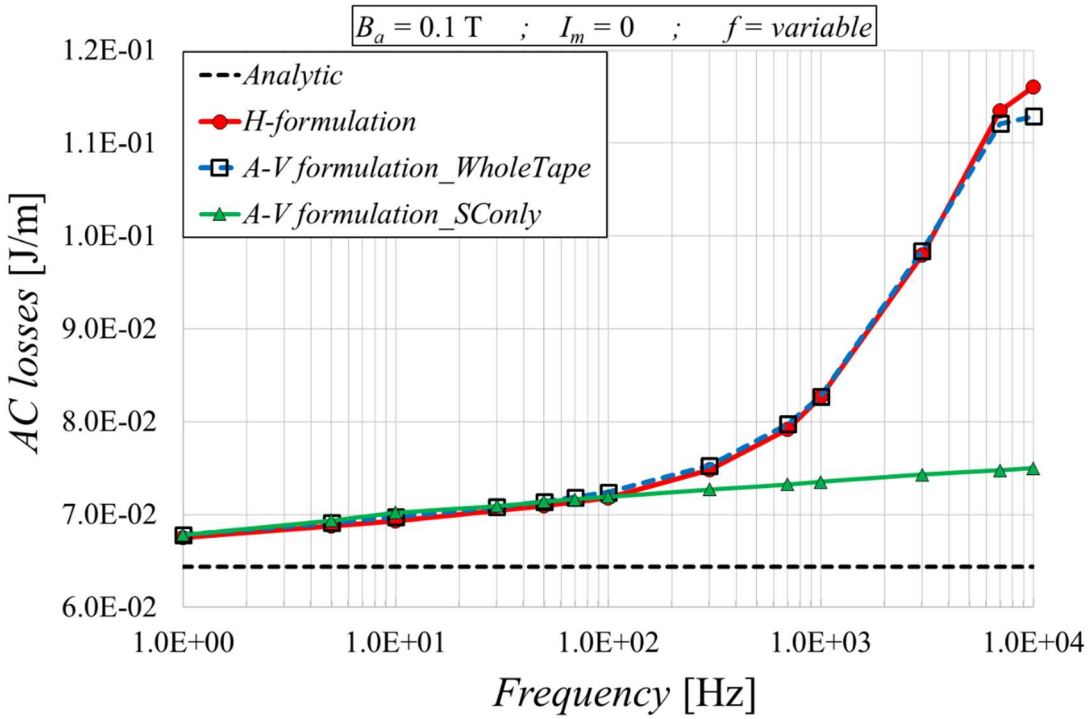

Figure 4. Magnetization losses in the *SuNAM SCN04* tape due to a perpendicular field, computed with different methodologies. The field frequency is varied and the amplitude is set to 0.1 T.

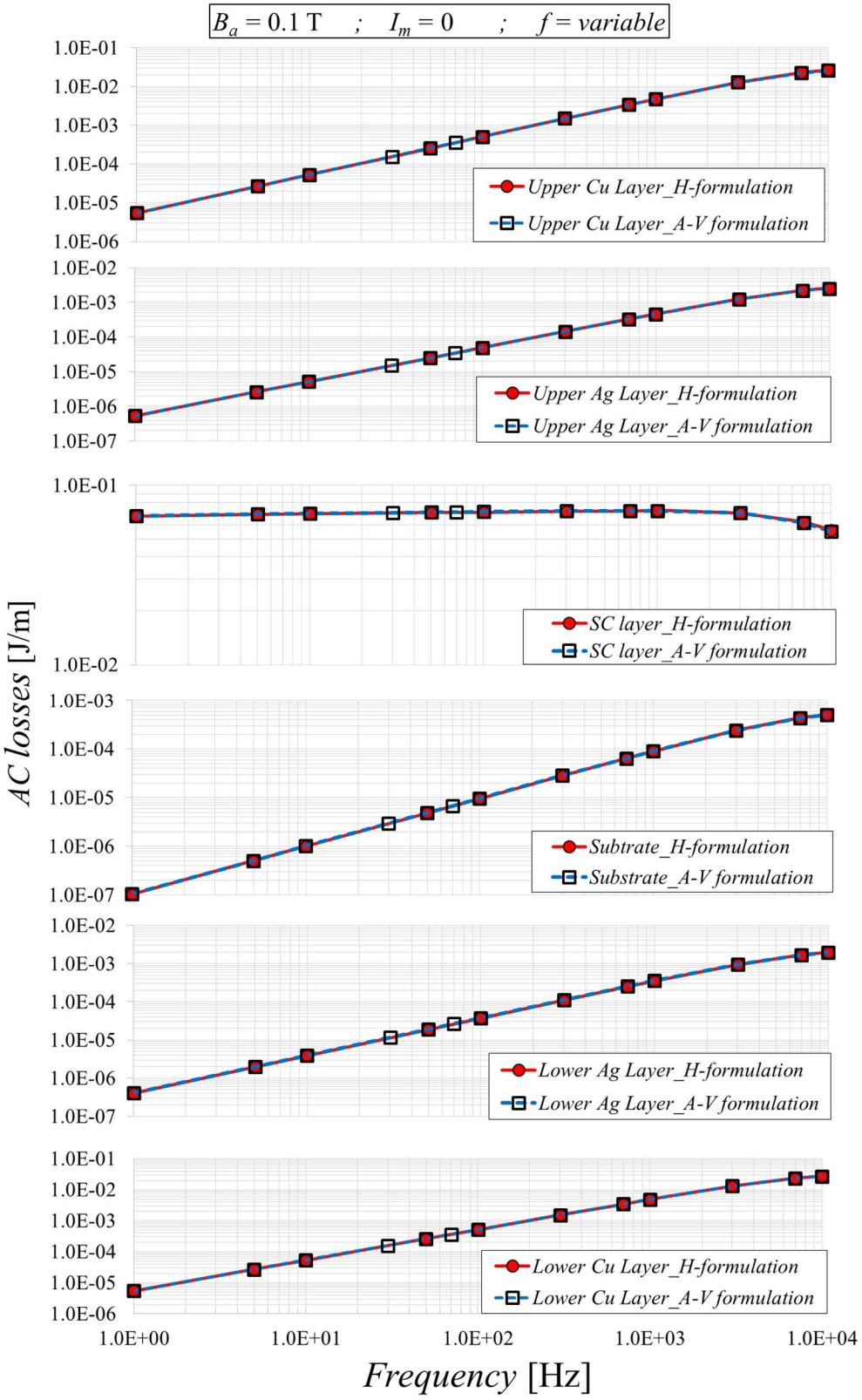

Figure 5. Magnetization losses in each layer of the *SuNAM SCN04* tape due to a perpendicular field, computed with different formulations. The field frequency is varied and the amplitude is set to 0.1 T.

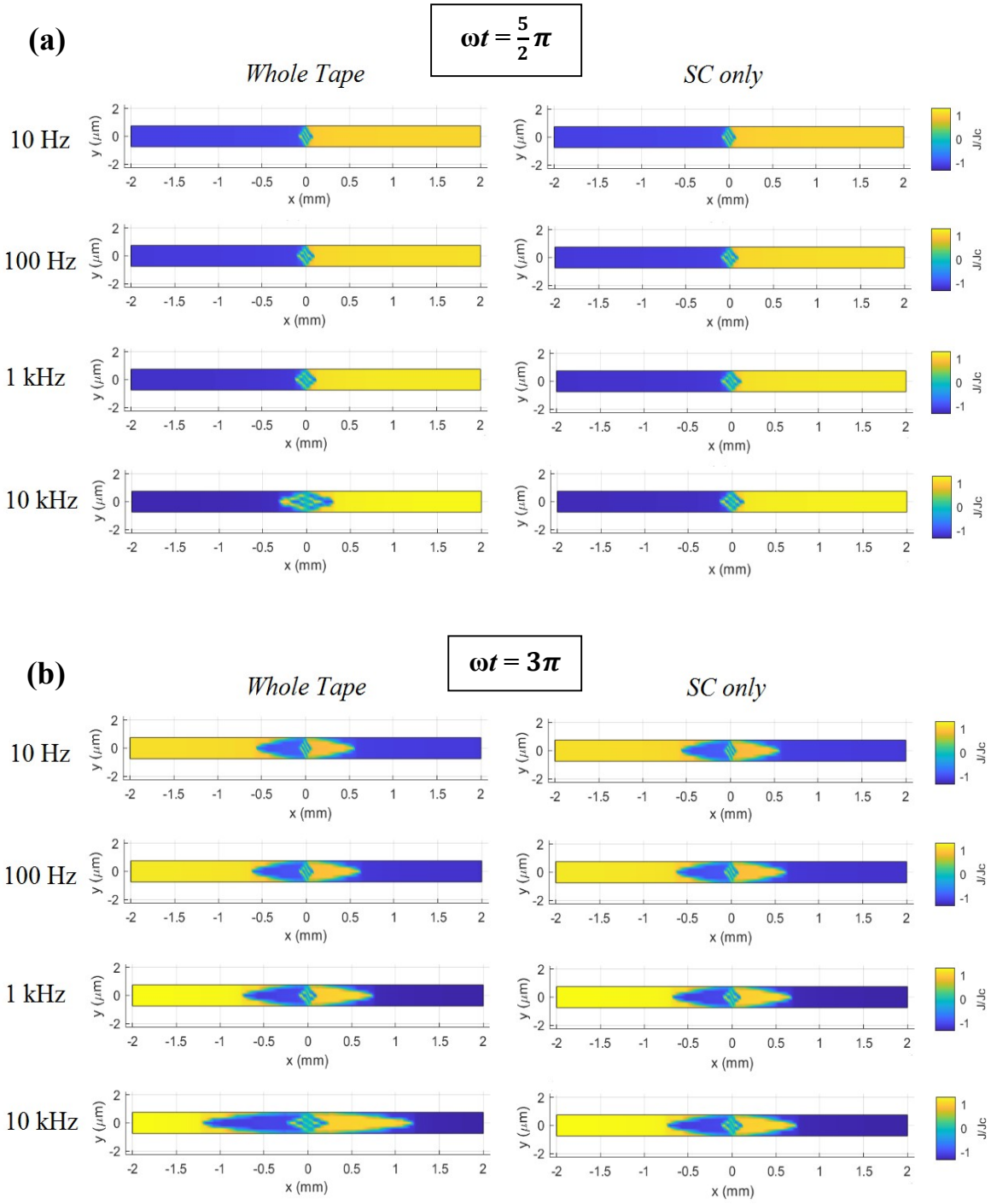

Figure 6. J/J_c distribution in the superconducting layer of the *SuNAM SCN04* tape subjected to a perpendicular magnetic field with an amplitude of 0.1 T and different frequencies, for $\omega t = \frac{5}{2}\pi$ (a) and $\omega t = 3\,\pi$ (b). In the left plots, the non-superconducting layers of the tape are included in the model, while in the right plots they are neglected.

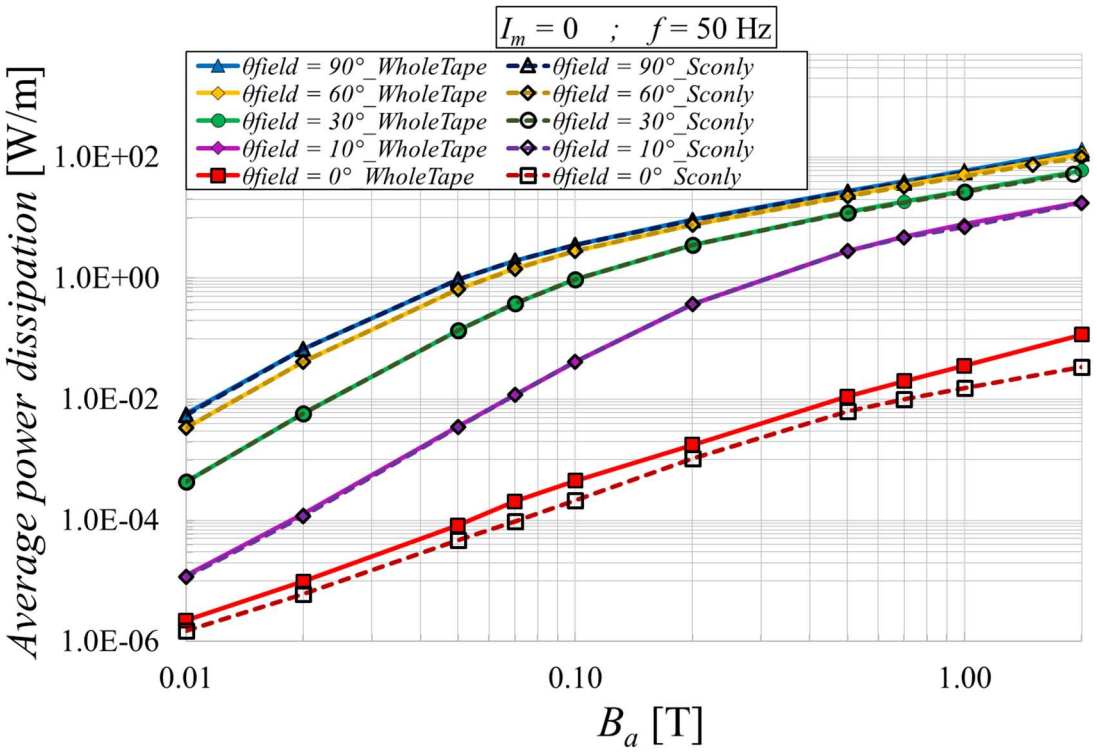

Figure 7. Average power dissipation computed for the *SuNAM SCN04* tape for a magnetic field applied with different orientations and amplitudes and $f = 50$ Hz.

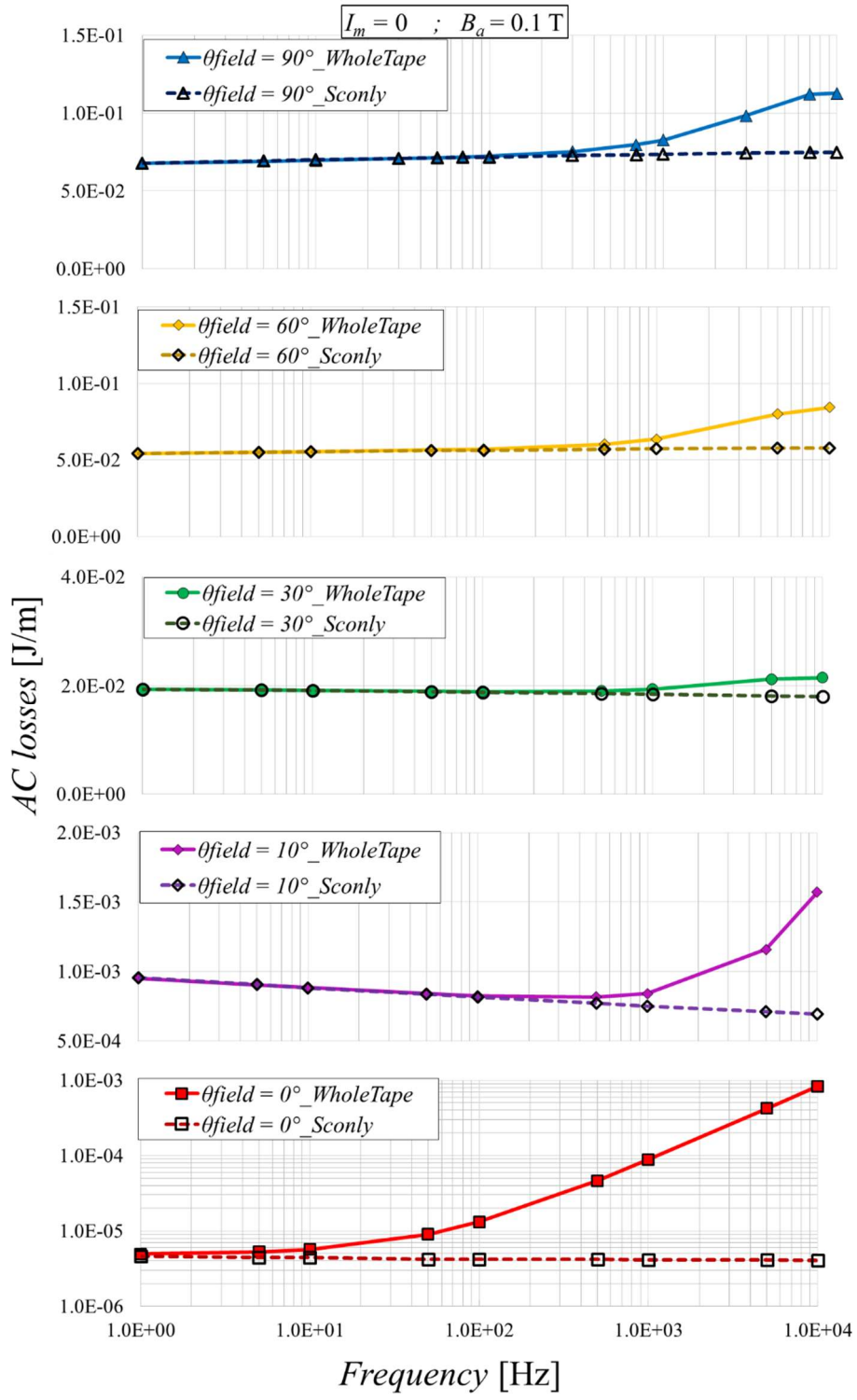

Figure 8. Magnetization losses in the *SuNAM SCN04* tape for a magnetic field with different orientations and frequencies and an amplitude of 0.1 T. The lower graph is in logarithmic scale while the upper ones are in semi-logarithmic scale.